RSC Advances

PAPER

View Article Online
View Journal | View Issue

Cite this: *RSC Adv.*, 2019, **9**, 29856

Development of a fused imidazo[1,2-*a*]pyridine based fluorescent probe for Fe^{3+} and Hg^{2+} in aqueous media and HeLa cells†

Suman Srivastava, *[a] Neha Thakur,[b] Ashutosh Singh,[d] Poonam Shukla,[c] Vipin Kumar Maikhuri,[c] Neha Garg,[d] Ashok Prasad[c] and Rampal Pandey *[b]

Received 24th June 2019
Accepted 15th September 2019

DOI: 10.1039/c9ra04743c

rsc.li/rsc-advances

A new fluorescent sensor **5** based on a fused imidazopyridine scaffold has been designed and synthesized *via* cascade cyclization. The reaction features the formation of three different C–N bonds in sequence. Imidazopyridine based fluorescent probe **5** exhibits highly sensitive and selective fluorescent sensing for Fe^{3+}('*turn-on*') and Hg^{2+}('*turn-off*'). The excellent selectivity of imidazopyridine for Fe^{3+}/Hg^{2+} was not hampered in the presence of any of the competing cations. The limit of detection (LOD) of **5** toward Fe^{3+} and Hg^{2+} has been estimated to be 4.0 ppb and 1.0 ppb, respectively, with a good linear relationship (R^2 = 0.99). Notably, **5** selectively detects Fe^{3+}/Hg^{2+} through fluorescence enhancement signalling both *in vitro* and in HeLa cells.

Introduction

The development of novel and synthetically feasible fluorescent sensors particularly for heavy metal ions (HTMs) is of growing interest because these metal ions are indispensable owing to their involvement in a variety of fundamental biological processes.[1] Iron is an essential trace element for both plants and animals, and plays an important role in cellular metabolism and enzyme catalysis.[2] On the other hand, mercury is known for its toxic effects, is widely distributed in the environment and bioaccumulates through the food chain.[3] To serve the purpose of sensing, different small molecule fluorescent probes have been developed for selective detection of iron (Fe^{3+})[4] and mercury (Hg^{2+}).[5,6] Further, reports dealing with the detection of HTMs under aqueous conditions or in a viable aqueous-ethanol media are rather scarce.[7–9]

In addition, imidazo[1,2-*a*]pyridine ring systems have fascinated a great deal of attention due to their biological activities, associated with the hybrid structure of imidazole and pyridine.[10] Imidazo[1,2-*a*]pyridine ring systems are also important in the field of material sciences,[11] because a few of the compounds belong to this class exhibit excited state intramolecular proton transfer (ESIPT) behavior.[12] Therefore, a large number of methodologies have been developed for the synthesis of imidazo[1,2-*a*]pyridine derivatives.[13] The immense applications of this class of compounds also prompted us to explore the synthetic methodologies for the preparation of fused imidazo[1,2-*a*]pyridines. Following our interest in the area of designing and synthesis of small bioactive molecule *via* ecofriendly route,[14] we report herein the synthesis, characterization and application of fused imidazopyridine compound for the detection of Fe^{3+} and Hg^{2+} in aqueous-alcoholic media. Notably, the systematic fluorescence intensity change can be associated to the detection ability for *in vitro* measurements however, sensing of analytes in cellular systems (inside biological cells) is a daunting task.[6b] Further, variation in fluorescence intensity in cellular systems may occur due to several other reasons.[6b,15,16]

Results and discussion

The imidazo[1,2-*a*]pyridines probe (**5**) was synthesized in three steps with overall yield 63%. Formylation of 4-methoxyacetophenone furnished 3-chloro-3-(4-methoxyphenyl) acrylaldehyde (**2**).[17] Sonogashira coupling of **2** with phenyl acetylene (**3a**) gives 2-(2-phenylethynyl) benzaldehyde (**4**).[18]

Condensation of *o*-phenylenediamine with **4** in DMF in presence of acetic acid under refluxing condition resulted in an oxidative cyclization to give desired probe 3-(4-methoxyphenyl)-1-phenylbenzo[4,5]imidazo[1,2-*a*]-pyridine, (**5**) (Scheme 1). Characterization of **5** has been done by NMR (^{1}H & ^{13}C), HRMS and single X-ray single crystal analysis. It is apparent from the mechanism that formation of **5** takes place by condensation cum cyclization as shown below (Scheme 2). Imine formation

[a]*Department of Applied Sciences, National Institute of Technology, Delhi, India. E-mail: sumanbhu08@gmail.com*

[b]*Department of Chemistry, National Institute of Technology Uttarakhand, India. E-mail: rppandeysu@gmail.com*

[c]*Department of Chemistry, University of Delhi, Delhi, India*

[d]*Indian Institute of Technology, Mandi, Himachal Pradesh, India*

† Electronic supplementary information (ESI) available. CCDC 1921596. For ESI and crystallographic data in CIF or other electronic format see DOI: 10.1039/c9ra04743c

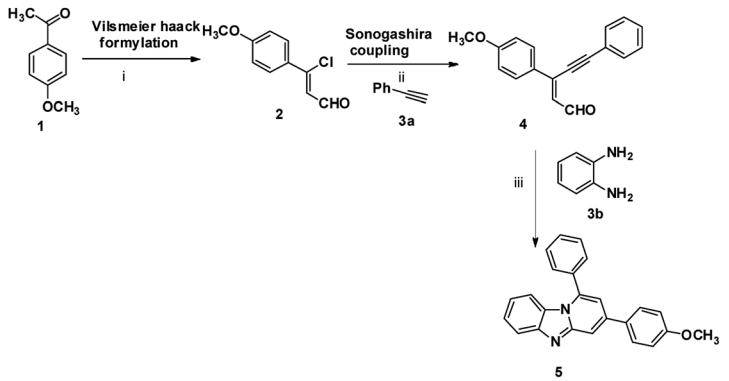

Scheme 1 Synthesis of imidazopyridine: (i) $POCl_3$, DMF, CH_3COONa, 0 °C to rt, 3 h; (ii) $PdCl_2(PPh_3)_3$, Et_3N, CH_3CN, rt, 5 h; (iii) DMF, acetic acid, 100 °C, 12 h, 63%.

followed by attack of amine nitrogen on imine carbon which leads to dihydrobenzimidazole (**4b**). Nitrogen atom of dihydrobenzimidazole attacks on alkynyl carbon as shown to obtain dihydrobenzimidazo pyridine (**4d**) after protonation. Oxidation of dihydrobenzimidazo pyridine (**4d**) yielded benzimidazo pyridine (**5**).

Structural descriptions

The structure of **5** has been authenticated by X-ray single crystal analysis (CCDC no. 1921596,† Fig. 1). It crystallizes in monoclinic system with space group '*P*121/*n*1'. The molecular planarity is an important factor for fluorescent probes. The molecular plane of **5** comprises imidazo[1,2-*a*]pyridine fluorophore whereas *p*-methoxyphenyl ring assumes twisted position in a way that half part lying above and half part lying below the molecular plane. The molecular plane also divides 1-phenyl substituent into two equal halves. The C–N, C–O and C–C bond lengths are within the normal ranges.[7] The twisting in *p*-methoxyphenyl ring measured through torsion angles calculated to be −27.70° (cisoid, C10–C9–C18–C23) and 154.80° (transoid, C10–C9–C18–C19). The phenyl ring assumes orientation perpendicular to the central pyridine ring. Probe **5** leads to the formation of 1D chain through edge-to-edge π···π stacking interaction which enables it to be a good candidate for dimer formation in the excited state (Fig. 1 and S7†).

Cation detection through absorption and fluorescence studies

The UV/vis spectrum of **5** displays absorption bands at 365, 326, 285 and 244 nm (pH, 7.2 in H_2O : EtOH, 8 : 2, v/v, at rt) (Fig. 2a). The low energy (LE) bands are assignable to the n–π* transitions and high energy bands may be attributed to the π–π* transitions.[7] Further, to assess the cation binding effect on absorption behavior of **5**, various alkali, alkaline and transition metal ions (5 equiv.; Na^+, K^+, Mg^{2+}, Ca^{2+}, Mn^{2+}, Fe^{2+}, Fe^{3+}, Co^{2+}, Ni^{2+}, Zn^{2+}, Ag^+, Cd^{2+} and Pb^{2+}; 10 mM) were added to the solutions of **5** (10 μM; 3 mL). Among tested cations, only Fe^{3+}

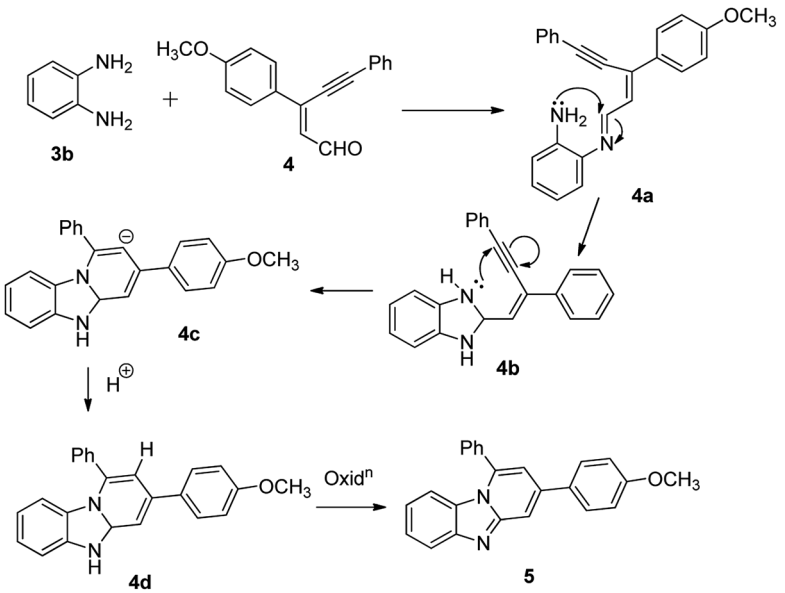

Scheme 2 Proposed mechanism for the formation of **5**.

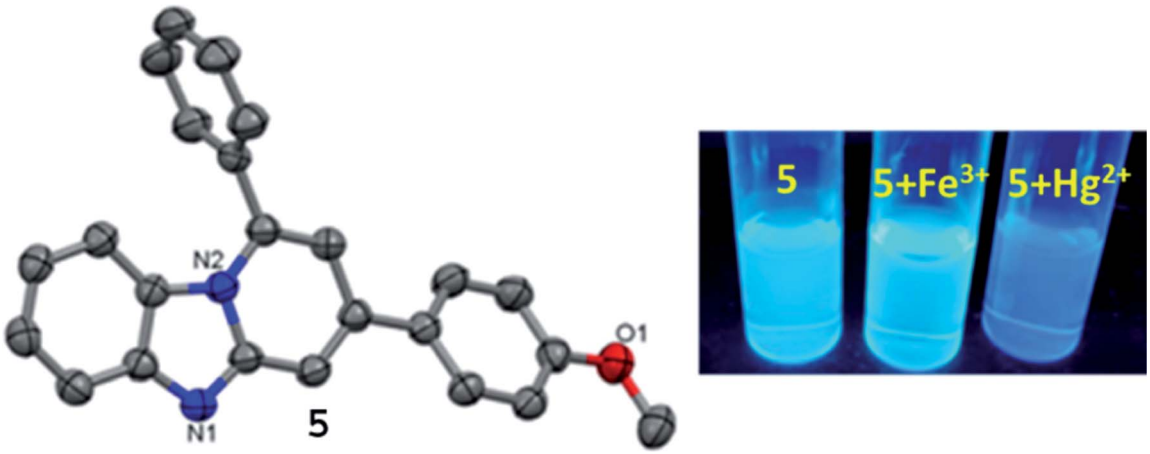

Fig. 1 (Left) X-ray single crystal structure of **5** (ellipsoidal probability 50%); (right) fluorescence image of **5** + Fe^{3+} and **5** + Hg^{2+} under UV-light (365 nm).

and Hg^{2+} induced significant changes in the spectral feature of **5** (Fig. S8†).

Addition of Fe^{3+} leads to the large hyperchromic shifts in both the LE bands however; hyperchromic shifts in the HE bands are relatively small to that of LE bands. In contrast, addition of Hg^{2+} to the solution of **5** causes ratiometric changes in the absorption bands through hyperchromic shifts in the LE bands and hypochromic shift in HE band along with appearance of a new band at 264 nm.

Considering substantial changes in the presence of Fe^{3+} and Hg^{2+} as well as to have deep insight about probe-cation binding, UV/vis titration studies were performed (Fig. 3). Gradual addition of Fe^{3+}(1.0 μL, 0.1 equiv.) to a solution of **5** leads to the noteworthy ratiometric change in the absorption bands through hyperchromic shift in the LE bands and hypochromic shift in the HE band (at 285 nm; ε, 22 769 M^{-1} cm^{-1}) (Fig. 3). Further, introducing more concentration of Fe^{3+}(2.0–15.0 μL) to the solution of **5** caused incessant hyperchromic shift in both the LE bands whereas HE bands become poorly structured with hyperchromic shifts at 244 nm and hypochromic shifts at 285 nm. Likewise, aliquot addition of Hg^{2+}(1.0 μL, 0.1 equiv.) to a solution of **5** induced significant ratiometric changes *via* hyperchromic shift at both the LE bands and hypochromic shift at 285 nm (ε, 31 686 M^{-1} cm^{-1}) whereas HE band at 244 nm is blue shifted to appear at 236 nm (Fig. 3). Further additions of Hg^{2+} (2.0–15.0 μL) lead to the similar ratiometric changes along with clear cut isosbestic points at 392, 306 and 245 nm, suggesting presence of more than two species in the medium. In addition, selectivity of **5** toward Fe^{3+} and Hg^{2+} was examined by introduction of Fe^{3+} (20 μL) to the solution of **5** followed by addition of Hg^{2+} (20 μL) to the same **5** + Fe^{3+} solution and the resultant **5** + Fe^{3+} + Hg^{2+} solution was left as such for an hour. Notably, spectral pattern of **5** + Fe^{3+} was almost completely altered to **5** + Hg^{2+} which strongly suggests better selectivity of **5** toward Hg^{2+} over Fe^{3+}.

Upon excitation at its LE band (λ_{ex}, 368 nm), **5** exhibits moderate fluorescence at 464 nm and the quantum yield (Φ_F) determined to be 0.37 (Fig. 2b).[8] The moderate Φ_F for **5** may be ascribed to the combined effect of intense LE absorption band and photoinduced electron transfer (PET).[8] Cation interaction behavior of **5** was also investigated through fluorescence spectral technique by individual and excessive addition of various cations (10 equiv.; 100 mM) to the solution of **5**. Notably, among introduced cations, only Fe^{3+} and Hg^{2+} could cause significant

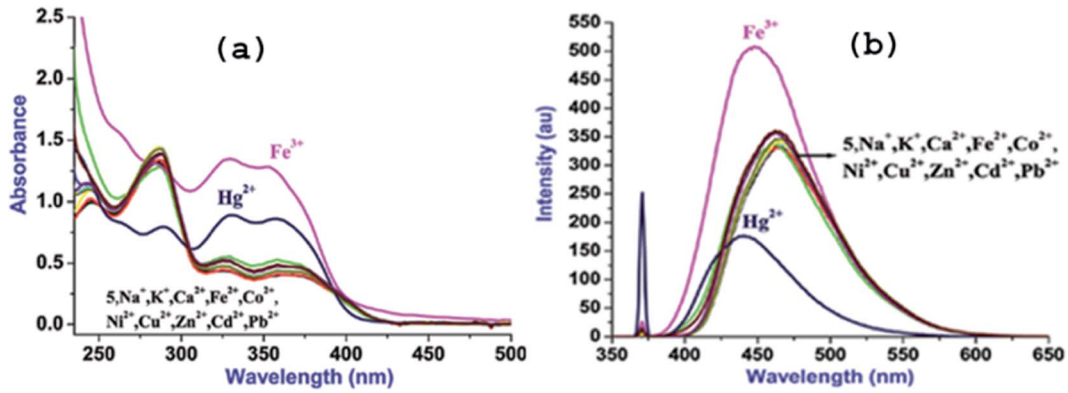

Fig. 2 UV/vis (a) and fluorescence (b) plots of **5** (10 μM, H_2O–EtOH, 8 : 2, v/v) in presence of various cations.

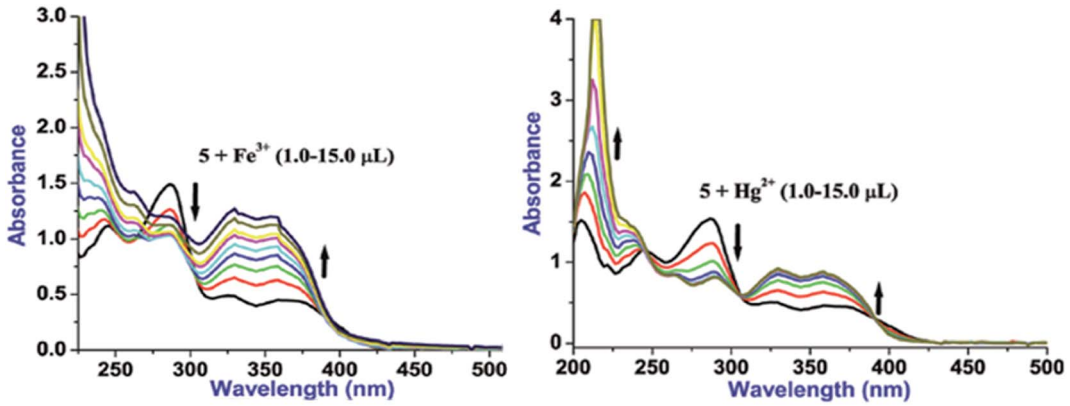

Fig. 3 UV/vis titration plots of **5** (10 μM, H_2O–EtOH, 8 : 2, v/v) with Fe^{3+} (left) and Hg^{2+} (right) ions.

fluorescence change whereas presence of other cations was futile in terms of the spectral change (Fig. 2b) which can be seen in the images taken both under natural conditions and UV-light (Fig. S8 ESI†).

Additions of both Fe^{3+} and Hg^{2+} lead to the subtle blue shift (820 cm^{-1} for Fe^{3+} and 1124 cm^{-1} for Hg^{2+}) however, Fe^{3+} induces 'turn-on' fluorescence and Hg^{2+} causes 'turn-off' fluorescence. To get profound idea into probe-cation binding, fluorescence titration studies were performed by gradual additions of Fe^{3+} and Hg^{2+} separately to the solution of **5** (Fig. 4). Aliquot additions of Fe^{3+} (1.0–15.0 μL) exhibited 'turn-on' fluorescence (~33%) with blue shifted emission maxima to

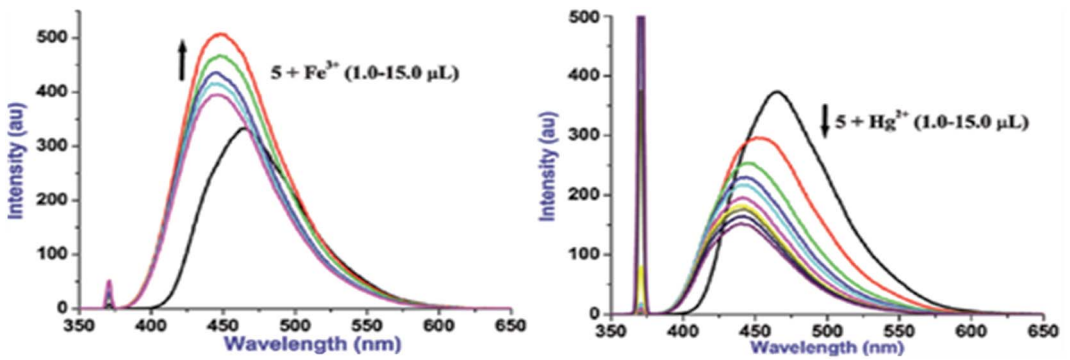

Fig. 4 Fluorescence titration plots of **5** (10 μM, H_2O–EtOH, 8 : 2, v/v) with Fe^{3+} (a) and Hg^{2+} (b) ions.

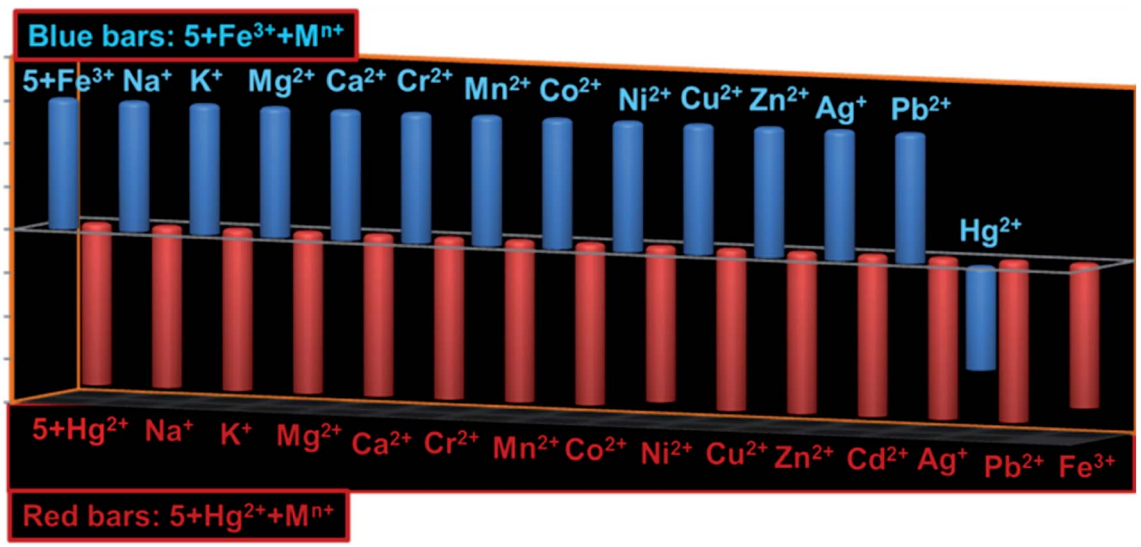

Fig. 5 Bar diagrams showing interference of various competing cations with fluorescence of **5** + Fe^{3+} (blue bars) and **5** + Hg^{2+} (brown bars).

appear at 447 nm. Likewise, gradual introduction of Hg^{2+}(1.0–15.0 μL) displayed 'turn-off' emission (~59%) with hypsochromically shifted fluorescence maxima to emerge at 441 nm. Blue shifts in case of both Fe^{3+} and Hg^{2+} suggest that probe **5** may be interacting with these cations through same binding site. Further, the 'turn-on' fluorescence of **5** upon binding with Fe^{3+} may be attributed to an increase in charge transfer from imidazo nitrogen of **5** to Fe^{3+} and/or due to chelation enhanced fluorescence (CHEF).[8] In contrast, 'turn-off' signaling with Hg^{2+} may be ascribed to the spin orbit coupling and/or the chelation-enhanced quenching (CHEQ) effect.[9]

The Job's plot analysis revealed 1 : 1 probe-cation stoichiometry for Fe^{3+} whereas 2 : 1 for Hg^{2+} (Fig. S9; ESI†). The quenching constant (K_{sv}) for **5** + Hg^{2+} has been determined to be 1.52×10^4 M^{-1} derived from the Stern–Volmer plot (Fig. S10; ESI†). Using Benesi–Hildebrand method, the association constants (K_a) for **5** + Fe^{3+} and **5** + Hg^{2+} were calculated to be 1.09×10^5 M^{-1} and 1.31×10^5 M^{-1}, respectively (Fig. S11; ESI†).[19] Moreover, the fluorescent detection of cations can only be claimed if competitive analytes induce insignificant interference to the selectivity assured by probe, therefore, we examined two sequences of interference: (1) various cations were successively added to the solution containing complex **5** + Fe^{3+} and/or **5** + Hg^{2+}; (2) Fe^{3+} and/or Hg^{2+} were added separately into the solution containing **5** + M^{n+} (M = various tested cations; (Fig. 5). Notably, none of the other metal ions could interfere to the selectivity of **5** toward Fe^{3+} and Hg^{2+}. Moreover, **5** offer greater selectivity for Hg^{2+} over Fe^{3+}. Other trivalent cations like Cr^{3+} and Al^{3+} could also not affect the selectivity assay of **5**.

The sensitivity of **5** (1.0 μM) toward Fe^{3+} and Hg^{2+} was examined in the concentration range of 10^{-12} M to 10^{-6} M wherein both the cations perturbed the fluorescence intensity of **5** at a concentration of 10^{-9} M. To further get better accuracy, 10^{-9} M ($1.0 \times 10^{-9} - 9.0 \times 10^{-9}$ M) concentration of Fe^{3+} and/

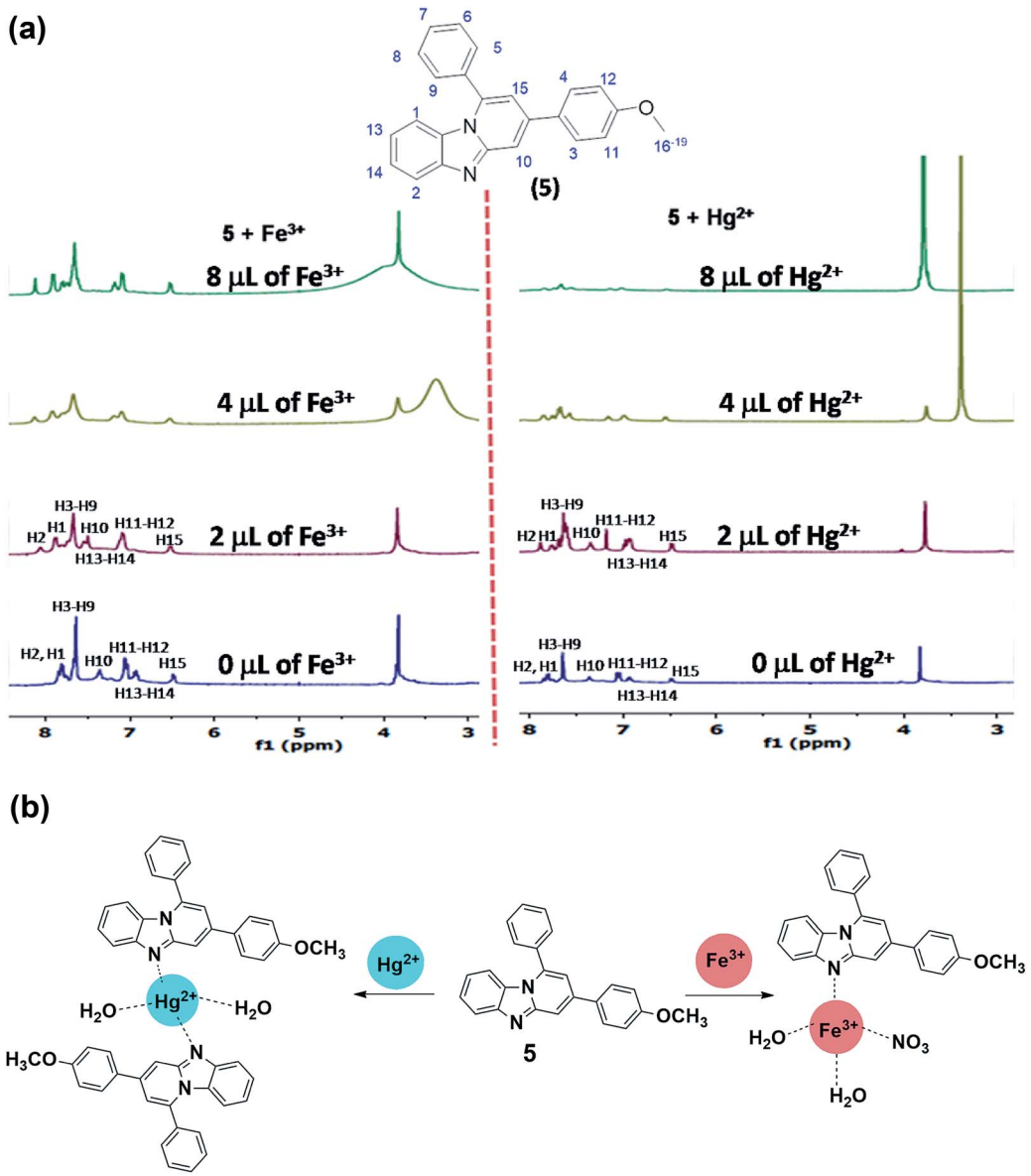

Fig. 6 (a) ^{1}H NMR titration plot of **5** with Fe^{3+} and Hg^{2+}; (b) Binding of probe **5** with Fe^{3+} and Hg^{2+} in aqueous-ethanol media.

or Hg^{2+} were introduced to the solution of **5** (1.0 μM) and displayed good plot linearity ($R^2 = 0.99$) with limit of detection (LOD) of 4.0 ppb (Fe^{3+}) and 1.0 ppb (Hg^{2+}) (Fig. S12; ESI†). It suggests that **5** can potentially be used as probe for practical detection of Fe^{3+} and Hg^{2+}. Further, **5** exhibited almost complete fluorescence revival upon excessive addition of EDTA (5.0 equivalent) to the solution of **5** + Fe^{3+}/Hg^{2+} suggesting that probe **5** can serve as reversible probe for said cations.

^{1}H NMR titration studies

The information about binding site of **5** for Fe^{3+} and Hg^{2+} cations was obtained though ^{1}H NMR titration studies (Fig. 6a) which show significant downfield shift in the protons adjacent to imidazo-nitrogen both in presence of Fe^{3+} and Hg^{2+}. Addition of Fe^{3+} (2.0 μL) to the solution of **5** led to the downfield shift in the aromatic protons H2 and H1 to appear at 8.11 ppm ($\Delta\delta$ = 0.27 ppm) and 7.94 ppm ($\Delta\delta$ = 0.10 ppm), respectively (Fig. 6a). Further addition of Fe^{3+} (4.0 μL) caused incessant downfield shift in H2 and H1 protons to resonate at 8.15 ppm ($\Delta\delta$ = 0.31 ppm) and Fe^{3+} and 8.07 ppm ($\Delta\delta$ = 0.23 ppm), respectively. Increasing the concentration of Fe^{3+} (4.0 μL) to the solution induced insignificant downfield shift to the resonances of **5**. Likewise, addition of Hg^{2+} (2.0 μL) to the solution of **5** resulted in the downfield shift to H2 and H1 aromatic protons to resonate at 8.02 ppm ($\Delta\delta$ = 0.18 ppm) and 7.89 ppm ($\Delta\delta$ = 0.05 ppm), respectively (Fig. 6a). Further additions of Hg^{2+} (4.0 μL) induced large downfield shift in H2 proton to appear at 8.29 ppm ($\Delta\delta$ = 0.45 ppm) whereas H1 proton resonates at 8.00 ppm ($\Delta\delta$ = 0.16 ppm). It is noteworthy to mention that –OCH_3 proton exhibits insignificant downfield shift in presence of Fe^{3+}/Hg^{2+}, which rules out the binding of cations through methoxy oxygen site. Overall, ^{1}H NMR titration spectra clearly displayed larger downfield shift for H2 proton (adjacent to the nitrogen donor site) relative to other aromatic protons and thereby strongly suggests imidazo-nitrogen as m downfield shift in presence of Fe^{3+}/Hg^{2+}, which rules out the binding of cations through methoxy oxygen site. Overall, ^{1}H NMR titration spectra clearly displayed larger downfield shift for H2 proton (adjacent to the nitrogen donor site) relative to other aromatic protons and thereby strongly suggests imidazo-nitrogen as most probable binding site for both the metal ions.

ESI-mass spectral studies

Further to get better idea about the complex ensued from probe-cation binding, ESI-MS spectra of compound obtained upon treatment of **5** with Hg^{2+} and Fe^{3+} salts, were acquired (Fig. S13; ESI†). The **5** + Hg^{2+} complex exhibits a peak at *m*/*z* 469 which corresponds to the half of the $[Hg(\mathbf{5})_2(H_2O)_2]^{2+}$ entity having at molecular mass of 938. As the charge (*z*) in Hg(II)-complex is +2, it displays $[M]^+/2$ peak at *m*/*z* 469 (938/2). Although, the base peak of Hg(II) complex is in accordance with the $[M + 1]^+$ peak of probe **5** (*m*/*z*,350). Likewise, **5** + Fe^{3+} complex shows moderately abundant $[M]^+/2$ peak at *m*/*z* 252 which is in accordance with half of the formula $[Fe(\mathbf{5})(NO_3)(H_2O)_2]^{2+}$ which have molecular mass of 504. Overall, the ESI-MS spectra also supported the probe-cation binding and stoichiometry (Fig. 6b).

Imaging in HeLa cells

To evaluate the feasibility of Fe^{3+} and Hg^{2+} sensing by **5** inside the cells, the HeLa cells were incubated with different concentration of the respective ions for 10 min. The phase contrast and blue channel images of the fixed cells after probing with sample is shown in Fig. 7. Overlay images showed that the blue fluorescence coincides with the cells. The blue channel displayed an

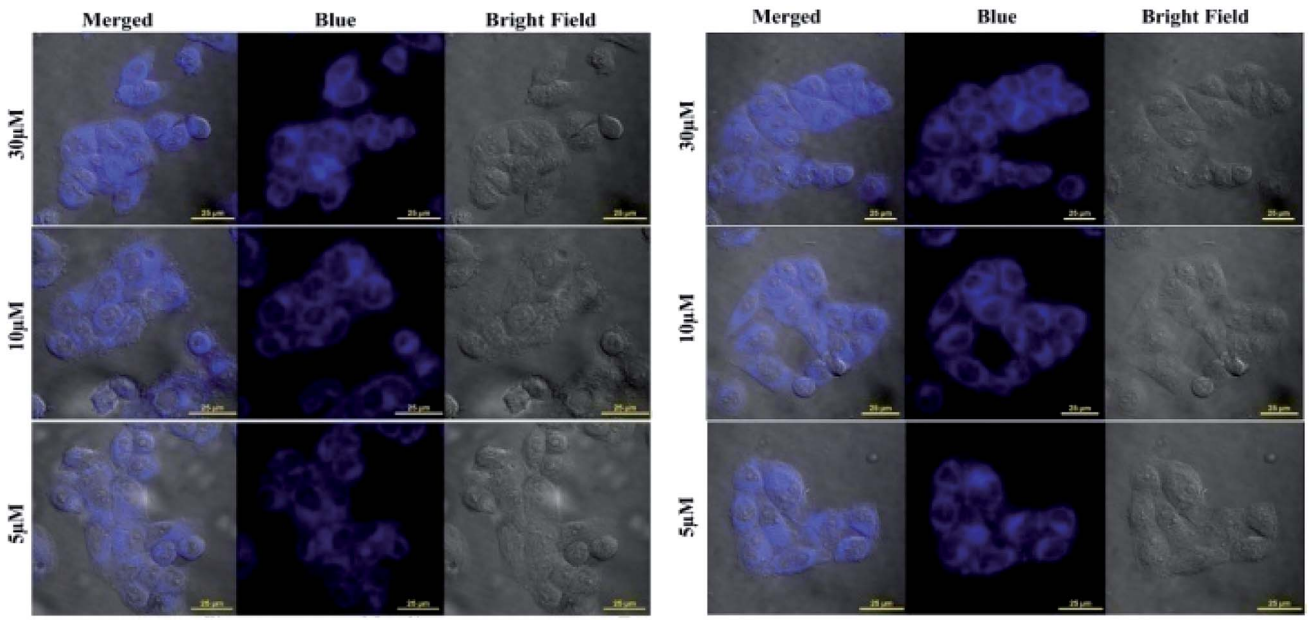

Fig. 7 Confocal images showing Fe^{3+} (left) and Hg^{2+} (right) sensing by **5** inside HeLa cells. The cells were incubated with increasing concentration of the respective ions.

increase in fluorescence with increasing concentration of both Fe^{3+} and Hg^{2+} and the same has been illustrated in the mean fluorescence intensity plot (Fig. S14 and S15; ESI†). Additionally, the cell morphology also indicated cell survival after 10 min of incubation with the respective ions. The sharp contrast in the confocal study indicates the efficient cellular uptake and micromolar sensing of Fe^{3+} and Hg^{2+} by **5**.

In summary, a fused imidazopyridine has been synthesized, thoroughly characterized and used as sensitive and highly selective fluorescent sensor for biologically and environmentally vital Fe^{3+} and Hg^{2+} through distinct fluorescence readout. Probe **5** was designed with the view point of having single open imidazolyl nitrogen as unique interaction site for cations so that none of the competing cation can interfere with its selectivity assay. The cation binding has been well examined and supported by UV/vis, fluorescence, ^{1}H NMR titration techniques and mass spectral studies. The ppb level sensitivity and quite high selectivity of **5** toward Fe^{3+} and Hg^{2+} strongly claimed its practical application for determination of Fe^{3+} and Hg^{2+} in biological/environmental samples. Eventually, imaging in HeLa cells incubated with **5** has revealed enhanced fluorescence for Fe^{3+} and Hg^{2+} ions which strongly supports the claim that **5** can potentially be used as fluorescent probe for these cations under cellular conditions.

Conflicts of interest

There are no conflicts to declare.

Acknowledgements

SS and RP acknowledge the Department of Science and Technology (DST) for financial support through Inspire Faculty Award No IFA-13-CH-123 and IFA12-CH-66 respectively. NG acknowledges Ramanujan Fellowship from SERB, India (SB/S2/RJN-072/2015) and BioX center and AMRC, IIT Mandi for providing facilities.

Notes and references

1 (*a*) K. P. Carter, A. M. Young and A. E. Palmer, *Chem. Rev.*, 2014, **114**(8), 4564–4601; (*b*) N. D. Acha, C. Elosúa, J. M. Corres and F. J. Arregui, *Sensors*, 2019, **19**(3), 599–633; (*c*) B. Kaur, N. Kaur and S. Kumar, *Coord. Chem. Rev.*, 2018, **358**, 13–69.

2 (*a*) R. Meneghini, *Free Radical Biol. Med.*, 1997, **23**, 783–792; (*b*) P. Aisen, M. Wessling-Resnick and E. A. Leibold, *Curr. Opin. Chem. Biol.*, 1999, **3**, 200–206; (*c*) R. S. Eisenstein, *Annu. Rev. Nutr.*, 2000, **20**, 627–662; (*d*) T. A. Rouault, *Nat. Chem. Biol.*, 2006, **2**, 406–414.

3 (*a*) F. D. Natale, A. Lancia, A. Molino, M. D. Natale, D. Karatza and D. Musmarra, *J. Hazard. Mater.*, 2006, **132**, 220–225; (*b*) C. M. L. Carvalho, E.-H. Chew, S. I. Hashemy, J. Lu and A. Holmgren, *J. Biol. Chem.*, 2008, **283**, 11913–11923; (*c*) W. F. Fitzgerald, C. H. Lamborg and C. R. Hammerschmidt, *Chem. Rev.*, 2007, **107**, 641–662.

4 (*a*) L. Zhang, J. Wang, J. Fan, K. Guo and X. Peng, *Bioorg. Med. Chem. Lett.*, 2011, **21**, 5413–5416; (*b*) J. Yao, W. Dou, W. Qin and W. Liu, *Inorg. Chem. Commun.*, 2009, **12**, 116–118; (*c*) Z.-X. Li, L.-F. Zhang, W.-Y. Zhao, X.-Y. Li, Y.-K. Guo, M.-M. Yu and J.-X. Liu, *Inorg. Chem. Commun.*, 2011, **14**, 1656–1658; (*d*) L.-J. Fan and W. E. Jones Jr, *J. Am. Chem. Soc.*, 2006, **128**, 6784–6785; (*e*) N. C. Lim, S. V. Pavlova and C. Bruckner, *Inorg. Chem.*, 2009, **48**, 1173–1182; (*f*) Y. Xiang and A. Tong, *Org. Lett.*, 2006, **8**, 1549–1552.

5 (*a*) H. N. Kim, W. X. Ren, J. S. Kim and J. Yoon, *Chem. Soc. Rev.*, 2012, **41**, 3210–3244 and references therein; (*b*) X. Chen, T. Pradhan, F. Wang, J. S. Kim and J. Yoon, *Chem. Rev.*, 2012, **112**, 1910–1956 and references therein; (*c*) H. N. Kim, M. H. Lee, H. J. Kim, J. S. Kim and J. Yoon, *Chem. Soc. Rev.*, 2008, **37**, 1465–1472 and references therein.

6 (*a*) J. Du, J. Fan, X. Peng, P. Sun, J. Wang, H. Li and S. Sun, *Org. Lett.*, 2010, **12**, 476–479; (*b*) S. Madhu, D. K. Sharma, S. K. Basu, S. Jadhav, A. Chowdhury and M. Ravikanth, *Inorg. Chem.*, 2013, **52**, 11136–11145; (*c*) X. Zhang, Y. Shiraishi and T. Hirai, *Tetrahedron Lett.*, 2008, **49**, 4178–4181.

7 (*a*) R. Pandey, G. Méhes, A. Kumar, R. K. Gupta, C. Adachi and D. S. Pandey, *Chem. Commun.*, 2014, **50**, 8032–8035; (*b*) R. Pandey, M. Yadav, M. Shahid, A. Misra and D. S. Pandey, *Tetrahedron Lett.*, 2012, **53**, 3550–3555.

8 (*a*) T. Nandhini, P. Kaleeswaran and K. Pitchumani, *Sens. Actuators, B*, 2016, **230**, 199–205; (*b*) R. Pandey, P. Kumar, A. K. Singh, M. Shahid, P.-z. Li, S. K. Singh, Q. Xu, A. Misra and D. S. Pandey, *Inorg. Chem.*, 2011, **50**, 3189–3197; (*c*) S. A. de Silva, A. Zavaleta, D. E. Baron, O. Allam, E. V. Isidor, N. Kashimura and J. M. Percarpio, *Tetrahedron Lett.*, 1997, **38**, 2237–2240.

9 (*a*) K. M. Vengaian, C. D. Britto, K. Sekar, G. Sivaraman and S. Singaravadivel, *RSC Adv.*, 2016, **6**, 7668–7673; (*b*) N. Thakur, M. D. Pandey and R. Pandey, *New J. Chem.*, 2018, **42**, 3582–3592; (*c*) R. Pandey, R. K. Gupta, M. Shahid, B. Maiti, A. Misra and D. S. Pandey, *Inorg. Chem.*, 2012, **51**, 298–311.

10 (*a*) F. Couty and G. Evano, in *Comprehensive Heterocyclic Chemistry III*, ed. A. R. Katritzky, C. A. Ramsden, E. F. V. Scriven and R. J. K. Taylor, Elsevier, Oxford, 2008, vol. 11, p. 409; (*b*) C. Enguehard-Gueiffier and A. Gueiffier, *Mini-Rev. Med. Chem.*, 2007, **7**, 888–899.

11 N. Shao, G. X. Pang, C. X. Yan, G. F. Shi and Y. Cheng, *J. Org. Chem.*, 2011, **76**, 7458–7465.

12 A. J. Stasyuk, M. Banasiewicz, M. K. Cyrański and D. T. Gryko, *J. Org. Chem.*, 2012, **77**, 5552–5558.

13 (*a*) A. K. Bagdi, S. Santra, K. Monir and A. Hajra, *Chem. Commun.*, 2015, **51**, 1555–1575; (*b*) A. K. Bagdi and A. Hajra, *Chem. Rec.*, 2016, **16**(4), 1868–1885.

14 (*a*) A. Kumar, S. Srivastava and G. Gupta, *Green Chem.*, 2012, **14**, 3269–3272; (*b*) A. Kumar, S. Srivastava, G. Gupta, V. Chaturvedi, S. Sinha and R. Srivastava, *ACS Comb. Sci.*, 2011, **13**, 65–71; (*c*) A. Kumar, S. Srivastava and G. Gupta, *Tetrahedron Lett.*, 2010, **51**, 517–520; (*d*) A. Kumar, S. Srivastava, G. Gupta, P. Kumar and J. Sarkar, *RSC Adv.*, 2013, **3**, 3548–3552; (*e*) S. Srivastava, *New J. Chem.*, 2019,

43, 6469–6471; (*f*) H. Sharma and S. Srivastava, *RSC Adv.*, 2018, **8**, 38974–38979.

15 (*a*) H. Giloh and J. W. Sedat, *Science*, 1982, **217**, 1252–1255; (*b*) D. Sinnecker, P. Voigt, N. Hellwig and M. Schaefer, *Biochemistry*, 2005, **44**, 7085–7094; (*c*) J. N. Henderson, H.-W. Ai, R. E. Campbell and S. J. Remington, *Proc. Natl. Acad. Sci. U. S. A.*, 2007, **104**, 6672–6677; (*d*) N. Periasamy, S. Bicknese and A. S. Verkman, *Photochem. Photobiol.*, 1996, **63**, 265–271.

16 (*a*) T. E. Kaiser, V. Stepanenko and F. Würthner, *J. Am. Chem. Soc.*, 2009, **131**, 6719–6732; (*b*) K.-R. Wang, D.-S. Guo, B.-P. Jiang, Z.-H. Sun and Y. Liu, *J. Phys. Chem. B*, 2010, **114**, 101–106.

17 P. H. J. Kouwer, W. F. Jager, W. J. Mijs and S. J. Picken, *Macromolecules*, 2002, **35**, 4322–4329.

18 (*a*) M. Gazvoda, M. Virant, B. Pinter and J. Košmrlj, *Nat. Commun.*, 2018, **9**, 4814–4822; (*b*) A. Chandra, B. Singh, S. Upadhyay and R. M. Singh, *Tetrahedron*, 2008, **64**, 11680–11685.

19 (*a*) K. A. Connors, *Binding Constants*, New York, Wiley, 1987; (*b*) S. H. Mashraqui, T. Khan, S. Sundaram, R. Betkar and M. Chandiramani, *Tetrahedron Lett.*, 2007, **48**, 8487–8490.